Acta Oceanol. Sin., 2020, Vol. 39, No. 3, P. 1–11
https://doi.org/10.1007/s13131-020-1538-8
http://www.hyxb.org.cn
E-mail: hyxbe@263.net

Characterization of longshore currents in southern East China Sea during summer and autumn

Peng Li[1], Benwei Shi[2]*, Yangang Li[1], Sijian Wang[1], Xin Lv[1], Yaping Wang[2], Qing Tian[3]

[1] Forecast Center for East China Sea, State Oceanic Administration, Shanghai 200136, China

[2] State Key Laboratory of Estuarine and Coastal Research, East China Normal University, Shanghai 200062, China

[3] School of Marine Sciences, Nanjing University of Information Science and Technology, Nanjing 210044, China

Received 15 June 2019; accepted 16 August 2019

Abstract

Current characteristics and vertical variations during summer and autumn in the southern East China Sea were investigated by measuring current profile, tide, wind, and wave data for 90 d from July 28 to October 25, 2015. Our results are: (1) The current was mainly a (clockwise) rotating flow, displaying reciprocating flow characteristics, and vertically the current directions were the same throughout the vertical profile. (2) The horizontal current speed was strongest during August (summer) with an average speed of 51.8 cm/s. The average current speeds during spring tides were highest in August and weakest in September, with speeds of 59.9 and 42.8 cm/s, respectively. (3) Considerable differences exist in average current speeds in different layers and seasons. The highest average current speeds were found in the middle–upper layers in August and in the middle–lower layers in September and October. (4) The residual current speed was highest in August, when the speed was 12.5–47.1 cm/s, whereas the vertical average current speed was 34.3 cm/s. The depth-averaged residual current speeds in September and October were only 50% of that in August, and the residual current direction gradually rotated in a counter-clockwise direction from the lower to surface layers. (5) Typhoon waves had a significant influence on the currents, and even affected the middle and lower water layers at depths of >70.0 m. Our results showed that the currents are controlled by the dynamic interplay of the Taiwan Warm Current, incursion of the Kuroshio Current onto the continental shelf, and monsoonal changes.

Key words: northeast Taiwan, ocean current, summer and autumn, typhoon

Citation: Li Peng, Shi Benwei, Li Yangang, Wang Sijian, Lv Xin, Wang Yaping, Tian Qing. 2020. Characterization of longshore currents in southern East China Sea during summer and autumn. Acta Oceanologica Sinica, 39(3): 1–11, doi: 10.1007/s13131-020-1538-8

1 Introduction

Offshore currents are responsible for the transportation of oceanic material, and influence physical, chemical, and biological processes in the oceans. As such, it is important to study the spatial and temporal variations in offshore currents to better understand environmental issues, pollution, and fishing activities in offshore regions (Liu et al., 2006; Gao and Wang, 2008; Rabouille et al., 2008).

The currents in the southeastern East China Sea are controlled mainly by the incursion of the Kuroshio Current and Taiwan Warm Current, which exhibit clear seasonal variability. These currents continuously transfer nutrients, water, and heat to the offshore China area, which influence the hydrology and ecology in China's coastal oceans (Su, 2001; Yu et al., 2002; Wang et al., 2006; Xiong, 2013). The Kuroshio Current originates from the southeast Philippines and is a branch of the Northern Equatorial Current, which flows north along the western edge of the North Pacific Ocean. The Kuroshio Current is warmer and more saline than the sea through which it flows. Where the Kuroshio Current flows through the offshore waters of the East China Sea, the main branch of the current flows along the Chinese continental shelf slope to the northeast, whereas another branch intrudes the East China Sea in the North Mien Hwa Canyon sea area off northeast Taiwan (Qiu and Imasato, 1990; Tang et al., 1999; Yang et al., 2011). However, the precise path of the current remains controversial (Su et al., 1987; Yang, 2011).

Zhao and Liu (2014) studied the seasonal variation in Kuroshio subsurface water intrusion onto the East China Sea continental shelf using conductivity–temperature–depth (CTD) data, and found that the intrusion strengthens in late spring, is strongest in summer, weakens in autumn, and weakest in winter. Interaction between the Kuroshio Current and the East China Sea continental shelf waters has been studied previously (Isobe et al., 2004; Xiong, 2013). Zhou et al. (2018) researched the intrusion of the Kuroshio subsurface water in the southern East China Sea and its variation in 2014 and 2015, and found that the Kuroshio subsurface water mainly intrudes onto the East China Sea shelf from northeast of Taiwan and bifurcates into a nearshore branch and an offshore branch. The research was based on field observation of dissolved inorganic iodine species and hydrographic data (temperature and salinity) to infer the he intrusion of the Kuroshio subsurface water in the southern East China, because lack of current observation, the further study on current characteristics of this area do not develop. Hu et al. (2008) and Yu et al. (2014)

Foundation item: The National Key Research and Development Program of China under contract No. 2016YFC1401207; the National Natural Science Foundation of China under contract No. 41625021; the Natural Science Foundation of Jiangsu Province under contract No. BK20170953.

*Corresponding author, E-mail: bwshi@sklec.ecnu.edu.cn

investigated the surface current field and seasonal variability in the Kuroshio and adjacent regions using satellite-tracked drifting buoy data. A nested high-resolution regional ocean numerical model has been used to evaluate seasonal variations in water, heat, and salt flux in the East China Sea and adjacent regions, revealing pronounced seasonal variations in water exchange (Qi et al., 2016). Bao et al. (2005) used an improved Princeton ocean model (POM) to simulate seasonal changes in continental shelf circulation in the East China Sea, and concluded that in winter the Kuroshio Current invades northward onto the continental shelf to the northeast Taiwan in the form of branches, but in summer enters onto the shelf from the north as a continental margin current. The Kuroshio intrusion onto the East China Sea is mainly due to the topographic beta spiral effect caused by changes in the topography of the northeastern waters of Taiwan (Yang et al., 2018). They first report the topographic beta spiral inferred from observation of temperature and salinity and numerical simulation method, but the contribution associated with the topographic beta spiral to the total transport of Kuroshio intrusion onto the East China Sea has not reached a conclusion.

The Taiwan Warm Current is located on the outer side of the Zhejiang–Fujian coastal currents, which form a typical monsoon circulation. Apart from its surface, which is affected by northerly winds in winter, the other layers move steadily northwards along 50–100 m isobaths, being stronger in summer and weaker in winter (Su, 2001). Water temperature and salinity data have been used to investigate the hydrological and chemical characteristics of the Taiwan Warm Current in summer, revealing that the current has two origins: Taiwan Strait water (surface waters) and Kuroshio subsurface water (deep waters) (Shi et al., 2013). These results are consistent with the findings of Guo et al. (1985). Zeng et al. (2012) studied temporal–spatial changes of the Zhejiang–Fujian coastal currents and Taiwan Warm Current during winter in southern Zhejiang using a bottom-mounted acoustic Doppler current profiler (ADCP). In the Taiwan Strait of the southern East China Sea, the current is strong and complex, and is influenced mainly by the monsoon and the Kuroshio Current. The speed and direction of the current exhibit significant seasonal variations (Ma, 2009). During winter in the eastern Taiwan Strait area, the Taiwan Strait current flows north along the west coast of Taiwan. The western and central areas of the Taiwan Strait are controlled by the southward-flowing Zhejiang–Fujian coastal currents. However, in summer the Taiwan Strait is dominated by the Taiwan Strait current to the northeast, and the current speed is greater than in winter (Ma, 2009). Lin et al. (2005) studied the characteristics of the Taiwan Strait current in winter using a bottom-mounted ADCP. Due to a lack of long-term hydrological observations, previous studies of the hydrodynamic environment in the northeastern Taiwan sea area relied on changes in water temperature and salinity structure (Isobe et al., 2004; Zhao and Liu, 2014; Zhang et al., 2017) or numerical simulations (Chao, 1990; Qiu and Imasato, 1990; Yang et al., 2011; Xiong, 2013).

Previous studies have mainly focused on the main branch of the Taiwan Warm Current, the main branch of the Kuroshio Current, and the lesser incursions of Kuroshio Current waters onto the continental shelf. However, few observational studies have examined the hydrodynamics northeast of Taiwan. As such, the purpose of this study was to analyze the hydrodynamic characteristics of currents in this region in summer and autumn. We conducted continuous observations of a vertical current profile, and tidal and meteorological conditions, from July 28 to October 25 2015 using a bottom-mounted ADCP and 10 m (in diameter and height) ocean-monitoring buoy. Our data provide a better understanding of the hydrological and ocean circulation in this region.

2 Data and methods

The observation station (26.04°N, 122.73°E) was located northeast of Taiwan, ~300 km from China's mainland, where the water depth is 106.0 m (Fig. 1). From July 28 to October 25, 2015, a bottom-mounted ADCP was deployed to continuously monitor the current and water pressure (i.e., sea level variations). Simultaneously, an observational buoy was used for continuous observation of wind speed and direction, waves, and atmospheric pressure at a site located 300 m from the ADCP. The bottom-mounted ADCP was installed in a drag-proof device and placed on the sea floor (~1.0 m above the sea bed) with sensors pointing upward. The 300 kHz ADCP (RD Instruments, USA) measures current speed and direction, and water pressure (i.e., water depth). It is operated with a blanking distance of 1.0 m, average sampling interval of 10 min, sampling duration of 1 min, cell size of 4.0 m, and 30 cells. The installation height of the sensor and blanking distance mean that the calculated height of the bottom layer is ~6.0 m above the seabed (96 m). The ADCP data playback indicated that the instrument was well positioned during the observation period, and that the inclination angles in the X and Y directions were < 5°. Due to the sea surface rising and falling with the tide, the depth of effective observation of the current profile changes with tidal level, and so there are different vertical observation layers (cells) at different times. Given the intensity of sound signal and pressure of the ADCP, we discarded the data upper 8m layer, and there were 23 effective observation layers. Thus, the surface and bottom layers were 8.0 and 96.0 m water depth, respectively.

The wind speed and direction were measured using an anemometer (05106; Young Enterprises, USA) installed on the equipment platform on top of the buoy (10.0 m above the sea surface), and the winds were sampled every hour. The wave sensor was constructed by the Institute of Oceanographic Instrumentation, Shandong Academy of Sciences, China. The wave sampling interval was 1.0 h, with a sampling time of 20 min, and with a sampling frequency 4 Hz. The wind and wave sensors on the buoy acquired data automatically, which were transferred to a coastal station (Forecast Center for East China Sea, State Oceanic Administration) via the BeiDou satellite. To analyze the seasonal variation in currents during summer and autumn, we selected the months of August (July 28 to August 26; 30 days), September (August 27 to September 25; 30 days), and October (September 26 to October 25; 30 days) to represent the summer, summer–autumn transition, and autumn seasons, respectively. Calculations of neap and spring tides are based on the average of two spring and two neap tides each month.

The calculated residual current during the observation period is the mixed residual current calculated from the vector synthesis method (all are closed tidal cycles). According to the current data, we separated the data into the north and east directions components. Then the components of the north and east directions are summed within a tide, so that the influence of the tidal current can be removed, and the rest is the residual current. Divide the sum value of north and east directions components by the length of observation period, the residual speed of north and east directions can be calculated. Thus, the speed and direction of the residual current can be calculated. The residual current is Euler residual current, which includes dense flow, wind-induced residual flow, and topographical residual flow. The residual current represents the direction of transport of the total water body

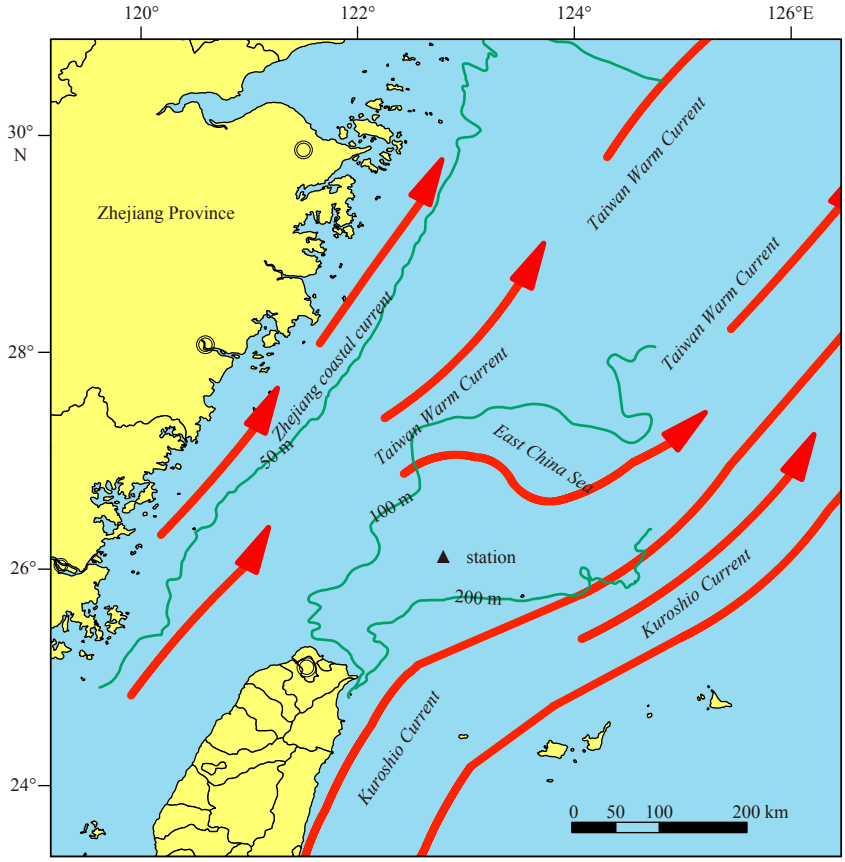

Fig. 1. Map of the study area showing the locations of gauging stations and coastal currents in summer (Su, 2001).

during the observation period.

3 Results

3.1 *Tidal characteristics*

During the observation period, the mean, maximum, and minimum tidal ranges were 1.21 m, 2.20 m, and 0.31 m, respectively. The mean tidal range during spring and neap tides was 1.66 m (weak tide area) and 0.73 m, respectively. Table 1 shows the results of the harmonic analysis of 24 dominant tidal constituents (Amplitude > 0.5 cm) at the 95% confidence level. These results show that semi-diurnal tides were the most significant constituent, followed by diurnal tides, which were much weaker than the former. Amongst these constituents, the amplitude of the M_2 tidal constituent (53.42 cm) was greatest, followed by the S_2 tidal constituent and the diurnal tidal constituents K_1 and O_1. The relative ratio (N_f) of the amplitudes of the diurnal and semi-diurnal tides ($N_f = (K_1 + O_1)/(M_2 + S_2)$) is 0.46, which is within the range of 0.25–0.50 corresponding to an irregular semi-diurnal tide (Defant, 1958).

The tide had a significant diurnal inequality (Fig. 2). The amplitude ratio of the S_2 to M_2 tidal constituents is 0.44, indicating that the diurnal inequality of the tide height is significant (>0.4) (Huang and Huang, 2005). The phase difference ($M_2 - (K_1 + O_1)$) between the semi-diurnal and diurnal tides is 188°. Phase differences of ~0°, ~180°, and ~270° correspond to high tide, low tide, and both high and low tide diurnal inequality, respectively (Huang and Huang, 2005). The phase difference of ~180° indicates a diurnal inequality in the low tide. Moreover, diurnal inequality of the tide during neap tides was more obvious with a range of ~0.6 m, and a maximum diurnal inequality of up to 0.86 m. The duration of ebb tides was slightly longer than that of flood tides, and the average durations of flood and ebb tides were 5 h 53 min and 6 h 33 min, respectively. From August 7 to 9, the water level fluctuation was between 10.0 and 15.0 cm, due to Typhoon Soudelor (Fig. 2).

3.2 *Current speed and direction*

The station was located in the open sea northeast of Taiwan. The current in this area is mainly a (clockwise) rotating flow, with reciprocating flow characteristics. The current direction was consistent along the vertical profile (Figs 3–5; for clarity only the

Table 1. Harmonic constituents of the tidal sea level (July 28 to October 25, 2015)

Tidal constituent	M_2	S_2	K_1	O_1	N_2	MM	Q_1	MU_2	NO_1	M_4	J_1	L_2
Amplitude/cm	53.42	23.73	18.33	17.4	12.61	4.65	2.8	2.75	2.64	1.63	1.52	1.33
Phase/(°)	221	248	227	182	205	51	166	140	222	329	259	303
Tidal constituent	MS_4	UPS_1	MN_4	SN_4	OO_1	M_6	ETA_2	MSF	$2MS_6$	$2O_1$	EPS_2	$2MN_6$
Amplitude/cm	1.16	1.05	1.03	0.98	0.86	0.81	0.77	0.73	0.29	0.59	0.51	0.50
Phase/(°)	24	58	316	21	325	174	282	94	233	259	110	166

transitions from spring to neap tides are plotted). There was a significant difference in current directions during ebb and flood tides. The flood current direction was to the north-northwest, with the direction being to the southeast (140°) at the beginning of the flood tide, which then rapidly turned to the north-northwest (330°) after ~20 min. During the whole flood period, the current direction was generally north-northwest, with a direction of 330°–360°, and the highest tidal water level was reached at a current direction of 360°. The flood tide direction at the beginning of the flood tide was the same as the current direction at the end of the ebb tide. The ebb tide direction was between 0° and 140° with a north direction at the beginning of the ebb tide. As the ebb tide proceeded, the current direction gradually rotated clockwise, and was ~140° at the lowest tidal water level. During medium tide, the current direction may be to the northeast and southeast in both flood and ebb tidal periods, oscillating over a range of 0° to 150°. In summer (August) and autumn (September–October) the current directions were similar, but the reciprocating flow characteristics were more significant in autumn than in summer (Figs 4–5).

The horizontal current speeds in the studied area are generally strong. Table 2 shows that the vertical average current speed varied considerably in the summer and autumn. The maximum average current speed of 51.8 cm/s occurred in August, compared with ~39.0 cm/s in September and October. The maximum current speeds during all months were >120.0 cm/s, which all occurred in the surface layer. The maximum current speed

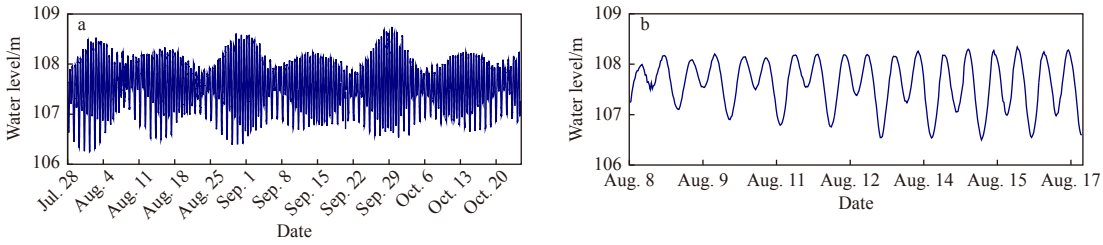

Fig. 2. Time-series of water level during the observation period (a) and typical periodicity of the water-level variation from neap to spring tides (b).

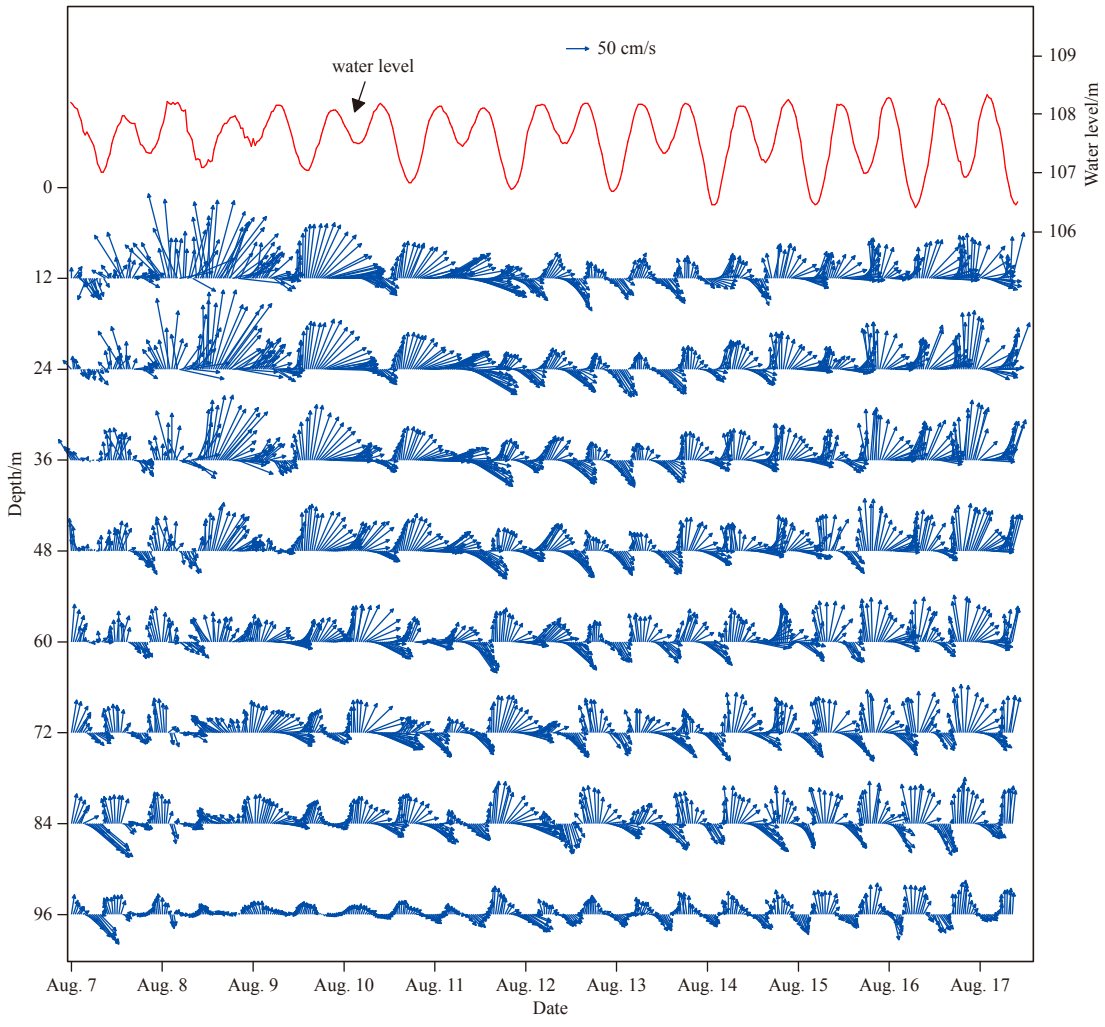

Fig. 3. Temporal variations in current vectors during August 2015.

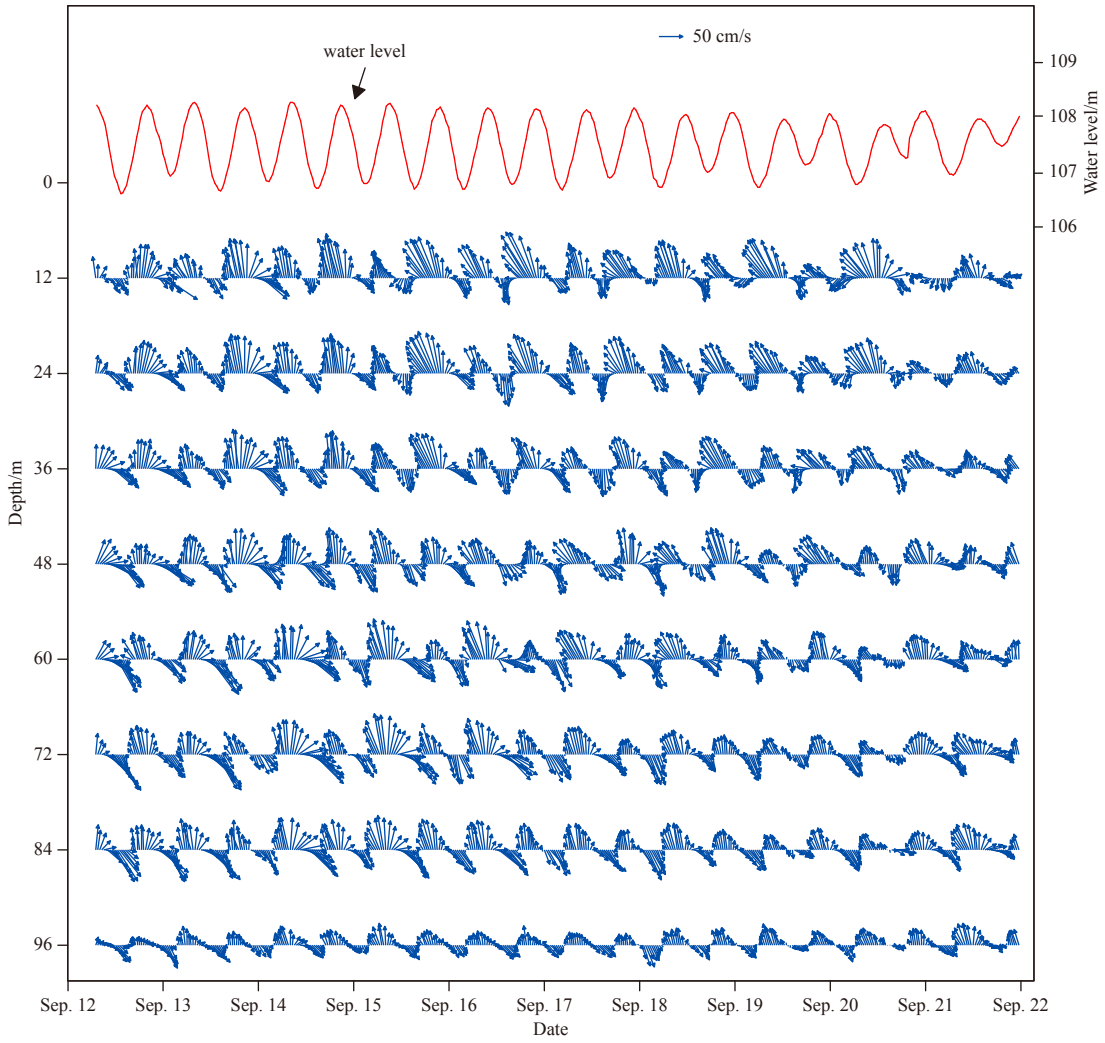

Fig. 4. Temporal variations in current vectors during September 2015.

reached 202.0 cm/s in August. The minimum current speeds were all <1.0 cm/s during slack tide. The average current speed during spring tides was highest in August and lowest in September, with speeds of 59.9 and 42.8 cm/s, respectively. During neap tides, the average current speeds were highest in August and slightly lower in September and October. In general, the average current speeds during spring tides were 1.5–1.7 times greater than those during neap tides.

In the vertical profile, the maximum current speeds during all the observation months were lowest in the bottom layer and highest in the surface layer (Fig. 6). The maximum current speeds in the bottom layer ranged from 56.8 cm/s (September) to 84.3 cm/s (October), and in the surface layer ranged from 127.0 to 202.0 cm/s. The maximum current speed in the surface layer was ~2.0 times greater than in the middle–lower water layers. Apart from the bottom and surface layers, the maximum current speeds were highest in August, lowest in September, and significantly higher in August than in September and October. The minimum current speed was <5.0 cm/s, and this did not vary through the vertical profile or seasonally.

The average current speeds varied among layers and seasons (Fig. 7). In August, the average current speed was lowest in the bottom layer (27.2 cm/s), rapidly increased from the bottom layer to the 88 m layer, and gradually increased thereafter to a maximum of 62.2 cm/s in 16 m layer. During spring tides, the average current speeds were lowest in the bottom layer. The vertical profile of average current speed has a convex shape in the middle–upper layers; the average current speeds were all >70.0 cm/s from the 16 m to 36 m layers. During neap tides, the average current speeds were lowest in the bottom layer and highest in the surface layer, and relatively constant in the middle layers from 16 m to 88 m layers (36.1–43.0 cm/s). The average current speeds during spring tides were 1.4–2.0 times those during neap tides in corresponding layers, and the vertical average of the current speeds during spring tides was 1.7 times that during neap tides.

In September, the vertical profile-shape of current speeds (monthly average, spring tide, and neap tide values) is similar. The minimum current speeds in different periods were all in the bottom layer (monthly average, spring tide, and neap tide values of 20.5, 21.3, and 20.1 cm/s, respectively). There were slight differences in the monthly average current speeds from the 8 m to 88 m layers of <10.0 cm/s. The vertical average of current speeds during spring tides was 1.5 times that during neap tides.

In October, the monthly average current speed was lowest in the bottom layer and highest in 72 m layer (56.7 cm/s). The monthly average current speed in the vertical profile was slightly higher in the middle–lower layers, with an average of 43.5 cm/s from the 64 m to 84 m layers. During spring tides, the vertical

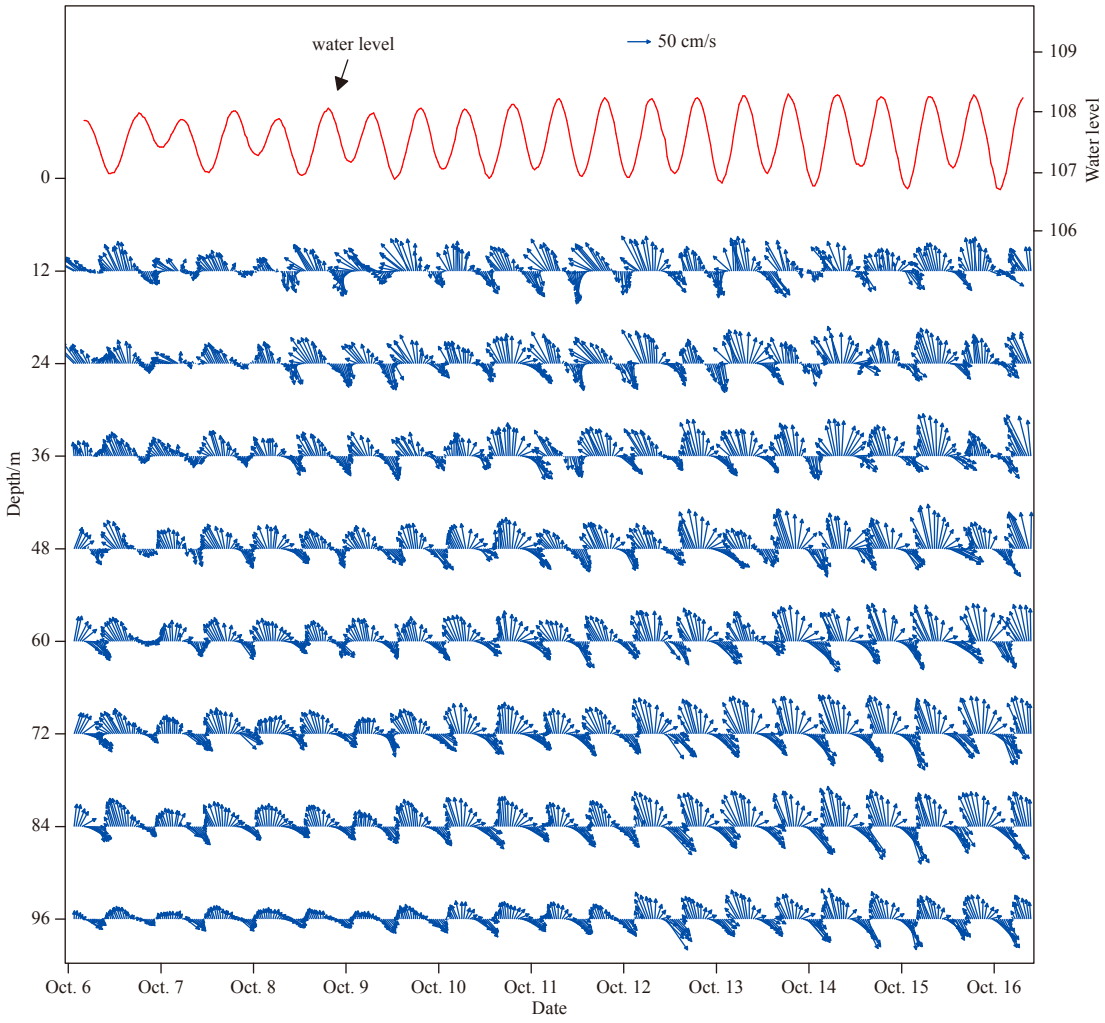

Fig. 5. Temporal variations in current vectors during October 2015.

Table 2. Characteristic average current speeds (cm/s) in the vertical profile

Time	Monthly average	Maximum	Minimum	Spring tide average	Neaptide average
August	51.8	202.0	0.3	59.9	35.8
September	38.7	141.4	0.2	42.8	28.7
October	39.7	127.0	0.2	47.3	28.8

profile of average current speeds has a clear convex shape in the middle–lower layers, with highest speeds in the 68 m to 80 m layers (>55.0 cm/s). The vertical average current profile during neap tides was similar during the whole month. The average current speed during spring tides was higher (by 1.5. to 2.2 times) than that during neap tides.

In general, apart from the bottom layers, the current speeds of given layers were highest in August and similar in September and October. The highest average current speeds during August were found in the middle–upper layers, and during September and October in the middle–lower layers.

3.3 *Residual current*

There were significant spatial and temporal variations in the residual current speed and direction (Fig. 8). The residual current direction varied by month of observation and with spring and neap tides. The residual current directions were generally to the northeast or north, but these varied among August, September, and October.

In August, the residual current directions were all to the northeast from the surface to bottom layers (34.1°–63.5°), and the directions were more consistent from the bottom to 64 m layers with an east-northeast direction (average=60.5°). In addition, there is a gradual counter-clockwise rotation of the direction from the 64 m to 8 m layers, with a direction of 38.3° in the 8 m layer. During spring and neap tides, the residual current directions were both to the northeast, but in given layers the currents during spring tides were rotated 15° counter-clockwise relative to those during neap tides.

In September, the residual currents were to the northeast or north. Below the 60 m layer, the residual current direction was to the east-northeast. From the 68 m to 72 m layers, the current direction was to the east (75.2°). The residual current directions rotated gradually counter-clockwise from the 60 m layer to the surface, being to the north in the 8 m layer. During spring tides, the residual current direction below the 44 m layer was to the east, whereas above this layer the current rotated gradually from the east to north-northwest in a counter-clockwise direction. During neap tides, the residual current direction rotated gradually in a

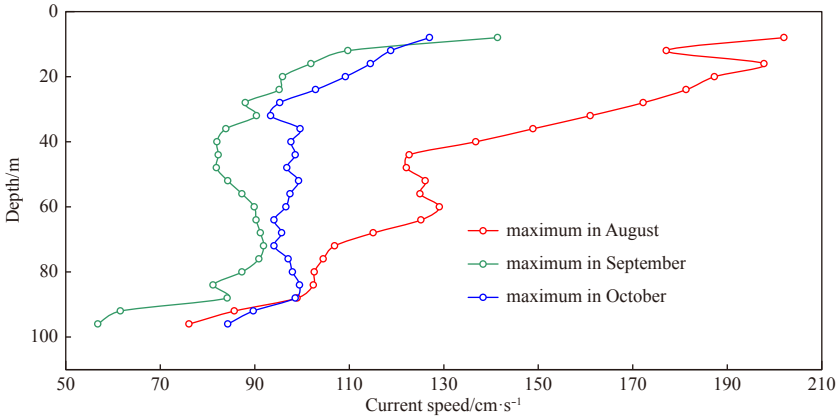

Fig. 6. Vertical variations in maximum current speed during the observation period.

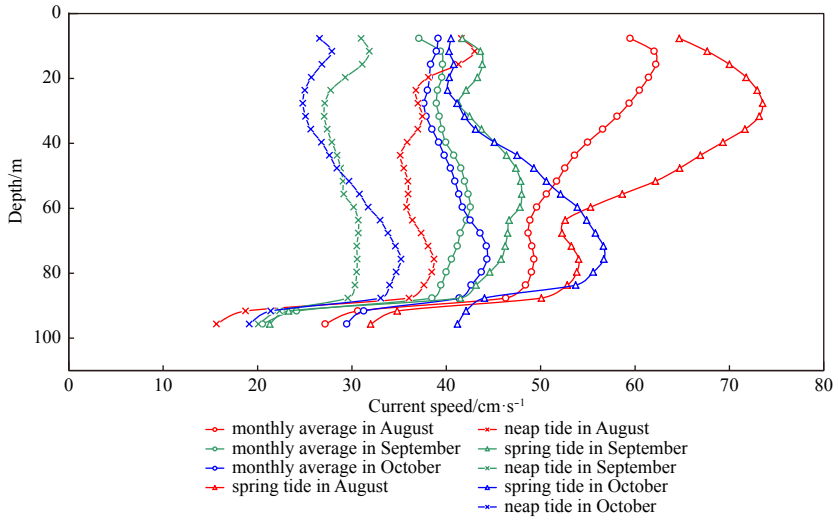

Fig. 7. Vertical variations in average current speed during the observation period.

counter-clockwise direction from the bottom to surface layers, and the direction was to the east-northeast in the bottom layer and to the north in the 44 m layer. The current direction was to the northwest above the 44 m layer.

In October, the residual current directions were to the northeast and north, similar to those in September (Fig. 9). In the bottom layer, the residual current direction was mostly to the east (60.2°). The residual current direction rotates gradually in a counter-clockwise direction from the bottom to surface layers, and was almost to the north in the 36 m layer. During spring tides, the residual current direction was 73° in the bottom layer, and the direction rotated gradually in a counter-clockwise direction from the bottom to surface layers, where the direction was to the north. During neap tides, the residual current direction from the bottom to surface layers also exhibited a counter-clockwise rotation, being to the northwest and northeast above and below the 52 m layer, respectively.

The residual current speed also exhibited significant temporal and vertical variations, being highest in August (12.5–47.1 cm/s; average=34.6 cm/s). The depth-averaged residual current speeds in September and October were only 50% of that in August. In August, the highest average speed of 47.1 cm/s was recorded in the 16 m layer and the lowest speed of 12.5 cm/s was recorded in the bottom layer. The current speed increased gradually from the bottom to upper layers, with the highest speed in the 12–16 m layers, which decreased slightly to 45.2 cm/s in the surface layer. The residual current speed during spring tides was higher than that during neap tides. During spring tides, the vertical average residual current speed was 42.8 cm/s, and the lowest speed was in the bottom layer (14.1 cm/s). The residual current speeds were highest in the middle–upper layers (average in the 24–36 m layers, >60.0 cm/s; Fig. 7). During neap tides, the difference in the vertical average residual current speeds was relatively small, and the vertical average residual current speed was 22.4 cm/s, although the speed in the upper layers (above the 22 m layer) was slightly higher.

In September, the vertical average residual current speed was 15.7 cm/s. The average residual current speed was lowest in the bottom layer (7.9 cm/s). From the surface to near-bottom layers, the range of residual current speeds was 10.1 to 19.4 cm/s. The highest speed was in the 56 m to 64 m layers (average=19.0 cm/s). The current speed gradually decreased above and below the 56–64 m layers. The vertical average residual current speed was 18.0 cm/s during spring tides, and was highest in the middle and lower layers, with the highest speed of 20.5 cm/s in the 52 m layer. During neap tides, the residual current speed was lower than

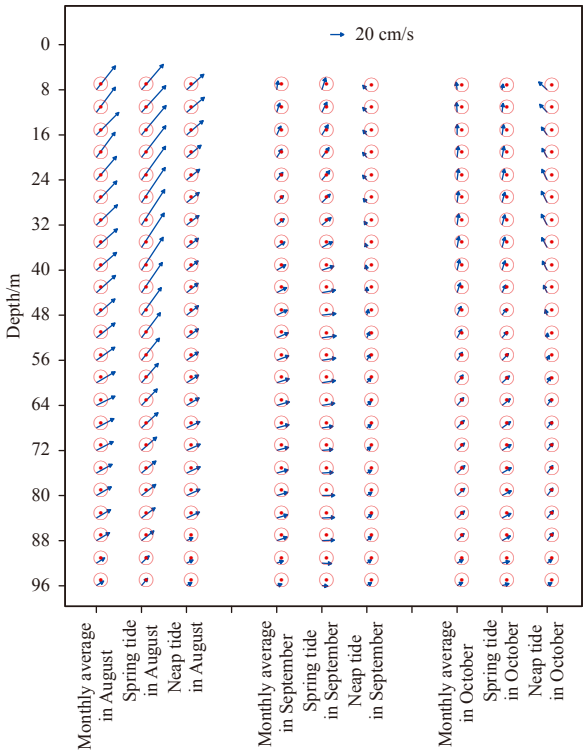

Fig. 8. Vertical variations in residual currents during the observation period.

that during spring tides, with a range of 6.8 to 10.2 cm/s.

In October, the vertical average residual current speed was 14.8 cm/s, and the vertical profile was similar to that in September. The residual current speed in the bottom layer was the lowest (9.6 cm/s), due to sea bed friction. Apart from the bottom layer, there was little difference in the residual current speeds (<5.0 cm/s) along the vertical profile. The current speeds were similar during spring and neap tides, with vertical averages of 14.2 and 13.3 cm/s, respectively. During spring tides, the differences in the residual current speed were small in the vertical direction. During neap tides, the residual current speed was lowest in the middle layer (6.8 cm/s in the 52 m layer).

4 Discussion

4.1 *Effects of the Taiwan Warm Current, Kuroshio Current, and monsoon on alongshore currents*

The Taiwan Warm Current is a typical monsoonal circulation current, although its surface waters are influenced by northerly winds in winter. As such, its subsurface current direction is to the northeast and changes little year-round. The Taiwan Warm Current flows steadily northward along the 50–100 m isobaths, and is stronger during summer and weaker during winter (Su, 2001). The flow of the Kuroshio Current intrusion onto the continental shelf of the East China Sea exhibits seasonal variations. The subsurface waters of the Kuroshio Current flow onto the continental shelf all year round, whereas the surface waters only flow onto the continental shelf in the second half of autumn and in winter (Su and Pan, 1990).

Given that the Taiwan Warm Current is strong in August, the current in the studied area is controlled mainly by the Taiwan Warm Current, but is also affected by the southwesterly monsoon. As such, the horizontal current speed and residual current speed were both much higher than the other months. The entire vertical profile of the sea in this region has a northeasterly residual current (46.3°) (Fig. 8). The vertical average residual current speed can reach 34.3 cm/s in August. Similarly, in the present study the horizontal current speed was highest in August (vertical average=51.8 cm/s). The maximum current speeds above the 84 m layer were all >100.0 cm/s (Fig. 3), despite there being no influence from typhoons. The highest average current speeds, particularly during spring tide, are in the middle–upper layers. The residual current exhibits the same characteristics as the average current.

In September, the summer monsoon winds gradually weaken, and the northeast monsoon gradually strengthens (Fig. 9). At the same time, the Taiwan Warm Current gradually weakens and the flow of the Kuroshio Current onto the continental shelf gradually strengthens (Su and Pan, 1990). Compared with August, the current speed decreases significantly in September with the vertical average current speed of 38.7 cm/s, and the current speed in the middle–upper layers decreases more significantly (Fig. 7). The direction of the residual current also changes in September, rotating counter-clockwise. The residual current direction in the middle–upper layers gradually rotates to the north-

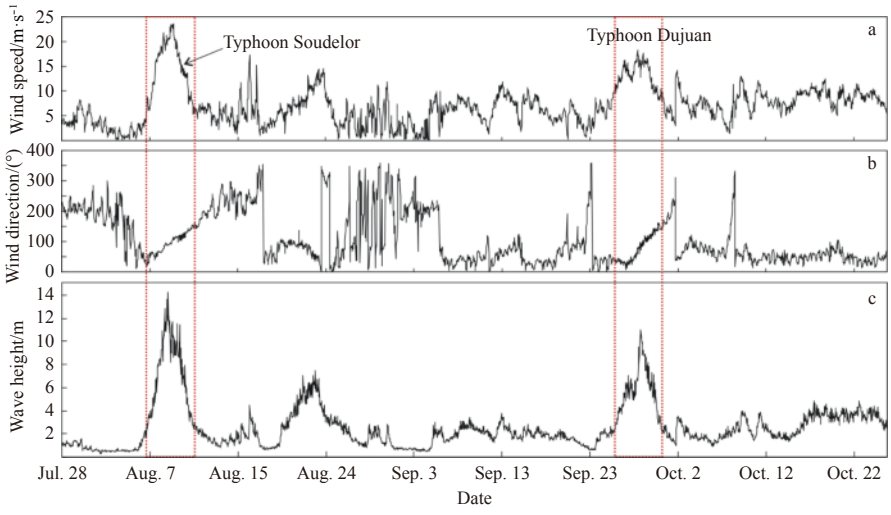

Fig. 9. Temporal variations in average wind speed, wind direction, and wave height during the observation period.

east and north, whereas in the layers above the 8 m layer the residual current direction is to the northwest. Due to the weak current during neap tides, the response of the current to the enhanced northeast monsoon and Kuroshio Current is more evident than during spring tides. In September, the residual current direction was already to the north and northwest above the 48 m layer (Fig. 8).

In October (autumn), the winter monsoon winds increase significantly, and the Taiwan Warm Current continues to weaken. Intrusion of the Kuroshio Current onto the continental shelf of the East China Sea continues to strengthen northeast of Taiwan (Yu et al., 2014), and this current has the greatest influence on the middle–lower layers (Shi et al., 2013). Our data show that the current speed increases in the middle–lower layers, particularly during spring tides. The highest average current speed was in the 68–80 m layers, reaching 56.2 cm/s during spring tides. Compared with September, the residual current direction continuously rotated counter-clockwise, while the monthly average residual current direction rotated to the north-northwest above the 32 m layer. During spring tides, the residual current was basically to the northeast, but this was slightly weaker than in September. Due to the lower current speed during neap tides, the current at these times was strongly influenced by monsoon strengthening and intrusion of the Kuroshio Current onto the continental shelf. As such, the residual current direction changed to the northwest above the 52 m layer and showed a slight increase in speed, which is consistent with the flood current direction (Fig. 8).

Yu et al. (2014) defined the boundary of the Kuroshio Current as a velocity transition between 20.0 and 30.0 cm/s, with the current speed in the main branch of the Kuroshio Current being >50.0 cm/s. In summer (June–August), the western Kuroshio Current in the East China Sea flows northward along the outer continental shelf. However, in autumn and winter, intrusion of the Kuroshio Current onto the continental shelf takes place. On the continental shelf of the East China Sea, the Taiwan Warm Current flows to the northeast year round, and is stronger in summer and weaker in winter, with speeds of 15.0–40.0 cm/s (Su and Pan, 1989). Our results are consistent with previously published research mentioned above. In August (summer), the vertical average residual current speed is 34.3 cm/s, which is greater than the current speed of the boundary of the Kuroshio Current, and similar to that of the Taiwan Warm Current, showing that the major hydrodynamic influence in this area during summer is the Taiwan Warm Current. The vertical average residual current speeds in September and October are 15.7 and 14.8 cm/s, respectively. These speeds are less than that of the boundary of the Kuroshio Current, and even less than that of the Taiwan Warm Current in winter. The residual current direction is more northward than that of the Taiwan Warm Current, and the highest current speed is in the middle–upper layers, particularly in October. This can be inferred to reflect the incursion of the Kuroshio Current onto the continental shelf.

The observation period (August–October) of our study covers the transition from summer to autumn. Our results reflect the seasonal characteristics of ocean currents in this region, and the combined influence of the monsoon, Taiwan Warm Current, and incursion flow of the Kuroshio Current onto the continental shelf. These results have important implications for the transport of water and heat, climate change, and the ecological setting in the East China Sea.

4.2 *Effects of sea conditions on alongshore currents*

Surface currents are affected by short-term wind conditions; however, during typhoons, waves can even affect the middle–lower water layers (depth=50–100 m; Harris et al., 2008). During the observation period, the studied area experienced two typhoons (Fig. 9). From August 7–9, 2015, the area was affected by Typhoon Soudelor (Fig. 9). On August 8, the 24 h average wind speed reached 20.3 m/s, and the maximum average wind speed was 24.2 m/s, with a maximum wind speed of 34.0 m/s. The wind direction gradually changed from northeast to southwest. The average of maximum wave height was 10.4 m, and the maximum wave height occurred at 8:00 on August 8 (wave height=14.2 m). From September 27–28, the studied area was affected by Typhoon Dujuan. The 24 h maximum average wind speed was 18.2 m/s, and the maximum wind speed reached 21.2 m/s. The maximum wave height was 10.7 m. According to previous studies, wave interaction does not take place until $d<0.25\times L$ (where d is the depth influenced by waves and L is wavelength) (Hallermeier, 1980). During Typhoon Soudelor, the wave period on August 8 ranged from 10.2 to 13.7 s and the average and maximum of wave periods were 11.6 and 13.7 s, respectively. Based on the widely used equation $L=gT^2/2\pi$ (where T is wave period and g=9.81 m/s^2; Woodroffe, 2003), the average wavelength in the study area would be 210.1 m and the maximum wavelength would be 293.0 m. As such, during Typhoon Soudelor the average depth impact by waves was 52.2 m, whereas the maximum depth influenced by waves was up to 73.3 m. Figure 3 shows how the continuous wind stress and waves during Typhoon Soudelor (Fig. 9) caused the current speeds above the 46 m layer to increase significantly. The 24 h average current speeds (August 8) above the 46 m layer were all >100.0 cm/s, although this was during neap tides (June 24 of the lunar calendar), and the average current speed was 1.8–2.4 times that of corresponding layers during spring tides. During the observation period, the maximum current speeds above and including the 72 m layer all occurred during Typhoon Soudelor (during neap tides), rather than during spring tides. However, the maximum current speeds below the 30 m layer all occurred during spring tides. Figure 6 shows how the maximum current speed above the 30 m layer increased rapidly in August, and was significantly greater than in September and October. As such, the typhoon waves influenced currents at depths of >70.0 m, which is consistent with the theoretical calculations. Compared with calmer conditions, the impact of typhoons on current direction was also significant, particularly in the surface and sub-surface layers. Given that the current in the study area is undergoing rotational flow, due to the influence of wind from a stable direction, the response of the current direction to the typhoon was complex (Fig. 3). However, the current above the 54 m layer exhibited unidirectional flow in part of the tidal period.

4.3 *Effects of tides on longshore currents*

Although our observation station was far from the mainland (~300 km), the effects of tides on the current are still significant. The mean tidal range was 1.21 m, and the maximum tidal range reached 2.2 m. Due to the large tidal range in this region, the tidal force is strong, resulting in a current that has apparent periodic variations from neap–spring tides and through individual tidal cycles in all layers. The average current speed during spring tides was 1.5–2.2 times that during neap tides. The difference between the current speed during spring and neap tides was greater in August than in September and October. Similarly, in August and September, the average residual current speeds during spring tides were >1.5 times those during neap tides. Although the studied region is located in the open sea, the current was characterized by significant reciprocating current behavior, which was to

the northwest and southeast during flood and ebb tides, respectively. Our results indicate that tides have a strong influence on the currents in this region.

5 Conclusions

Based on three months (August–October 2015) of continuous data acquisition of currents, water levels, winds, and waves northeast of Taiwan, the following main conclusions are drawn.

(1) An irregular semi-diurnal tide characterizes the studied area. The duration of ebb tides was slightly longer than that of flood tides. The area exhibits low tide diurnal daily inequality in the low tide, which is more pronounced during neap tides.

(2) The current is mainly a (clockwise) rotating flow that shows reciprocating flow characteristics. The flood current direction is to the north-northwest, whereas the ebb tide direction is to the east-southeast. The current directions are consistent through the vertical profile.

(3) Our results reflect the seasonal characteristics of ocean currents during summer and autumn in the area northeast of Taiwan, which are controlled by the Taiwan Warm Current, incursion of the Kuroshio Current onto the continental shelf, and the monsoon. In August, the current was mainly controlled by the Taiwan warm current, and the current was strongest. In September, the current speed decreases by 50% compared with August, and the direction of the residual current rotates counter-clockwise in the middle–upper layers to the northeast and north. Incursion of the Kuroshio Current onto the continental shelf of the East China Sea continues to strengthen in October. The residual current direction rotates counter-clockwise from the bottom (apart from the bottom layer) to the surface layers, and the current directions of the upper–middle layers are to the north or even northwest. This finding presumably has implications for understanding of sediment suspended transport in the Zhejiang coastal sea.

(4) During calm weather conditions, sea conditions generally only affect the current in the surface layer (depths<10 m), whereas during typhoons the waves can affect middle–lower water layers at depths of >70.0 m. Such effects led to the maximum current speed during the observation period. Our study therefore highlights the great effect of typhoons events on the entire water body.

References

Bao Xianwen, Lin Xiaopei, Wu Dexing, et al. 2005. Simulation and analysis of shelf circulation and its seasonal variability in the East China Sea. Journal of Ocean University of Qingdao (in Chinese), 35(3): 349–356

Chao S Y. 1990. Circulation of the East China Sea, a numerical study. Journal of Oceanography, 46(6): 273–295, doi: 10.1007/BF02123503

Defant A. 1958. Ebb and Flow: the Tides of Earth, Air, and Water. Ann Arbor: Michigan U P; Mayflower Publishing Co, 121

Gao Shu, Wang, Yaping. 2008. Changes in material fluxes from the Changjiang River and their implications on the adjoining continental shelf ecosystem. Continental Shelf Research, 28(12): 1490–1500, doi: 10.1016/j.csr.2007.02.010

Guo Binghuo, Lin Kui, Song Wanxian. 1985. Some problem s on the flow in the southern East China Sea in summer. Haiyang Xuebao (in Chinese), 7(2): 143–153

Hallermeier R. 1980. Sand motion initiation by water waves: two asymptotes. Journal of Waterways, Port, Coastal and Ocean Division, 106(3): 299–318

Harris C K, Sherwood C R, Signell R P, et al. 2008. Sediment dispersal in the northwestern Adriatic Sea. Journal of Geophysical Research: Oceans, 113(C11): C11S03, doi: 10.1029/2006JC003868

Hu Xiaomin, Xiong Xuejun, Qiao Fangli, et al. 2008. Surface current field and seasonal variability in the Kuroshio and adjacent regions derived from satellite-tracked drifter data. Haiyang Xuebao (in Chinese), 30(6): 1–16

Huang Zuke, Huang Lei. 2005. Tidal Theory and Calculation (in Chinese). Qingdao: China Ocean University Press, 293

Isobe A, Fujiwara E, Chang P H, et al. 2004. Intrusion of less saline shelf water into the Kuroshio subsurface layer in the East China Sea. Journal of Oceanography, 60(5): 853–863, doi: 10.1007/s10872-005-5778-1

Lin S F, Tang T Y, Jan S, et al. 2005. Taiwan strait current in winter. Continental Shelf Research, 25(9): 1023–1042, doi: 10.1016/j.csr.2004.12.008

Liu J P, Li A C, Xu K H, et al. 2006. Sedimentary features of the Yangtze River-derived along-shelf clinoform deposit in the East China Sea. Continental Shelf Research, 26(17–18): 2141–2156, doi: 10.1016/j.csr.2006.07.013

Ma Chao. 2009. The variability of the Kuroshio and its effects on the current in the Taiwan strait (in Chinese) [dissertation]. Qingdao: Ocean University of China

Qi Jifeng, Yin Baoshu, Zhang Qilong, et al. 2016. Seasonal variation of the volume, heat and salt transport in the East China Sea and adjacent regions. Haiyang Xuebao (in Chinese), 38(11): 1–19

Qiu Bo, Imasato N. 1990. A numerical study on the formation of the Kuroshio Counter Current and the Kuroshio Branch Current in the East China Sea. Continental Shelf Research, 10(2): 165–184, doi: 10.1016/0278-4343(90)90028-K

Rabouille C, Conley D J, Dai M H, et al. 2008. Comparison of hypoxia among four river-dominated ocean margins: the Changjiang (Yangtze), Mississippi, Pearl, and Rhone rivers. Continental Shelf Research, 28(12): 1527–1537, doi: 10.1016/j.csr.2008.01.020

Shi Xiaoyong, Li Hongmei, Wang Hao, et al. 2013. Taiwan warm current and its impact on the areas of frequent harmful alga bloom in the East China Sea in summer. Oceanologia et Limnologia Sinica (in Chinese), 44(5): 1208–1215

Su Jilan, Pan Yuqiu. 1987. On the shelf circulation north of Taiwan. Acta Oceanologica Sinica, 6(S1): 1–20

Su Jilan, Pan Yuqiu. 1989. A preliminary study of shelf circulation dynamics north of Taiwan. Haiyang Xuebao (in Chinese), 11(1): 1–14

Su Jilan, Pan Yuqiu. 1990. Discussion on the current path of the Kuroshio Intrusion Into Shelf Area.In: The Kuroshio Survey Research Papers (II) (in Chinese). Beijing: China Ocean Press, 187–197

Su Jilan. 2001. A review of circulation dynamics of the coastal oceans near China. Haiyang Xuebao (in Chinese), 23(4): 1–16

Tang T Y, Hsueh Y, Yang Y J, et al. 1999. Continental slope flow northeast of Taiwan. Journal of Physical Oceanography, 29(6): 1353–1362, doi: 10.1175/1520-0485(1999)029<1353:CSFNOT>2.0.CO;2

Wang Yaping, Pan Shaoming, Wang H V, et al. 2006. Measurements and analysis of water discharges and suspended sediment fluxes in Changjiang Estuary. Haiyang Xuebao (in Chinese), 61(1): 35–46

Woodroffe C D. 2003. Coasts: Form, Process and Evolution. Cambridge: Cambridge University Press

Xiong Xuejun. 2013. The circulation structure and mechanism studies on the China seas (in Chinese) [dissertation]. Qingdao: Ocean University of China, 224

Yang Dezhou. 2011. Numerical study on the Kuroshio intrusion on the East China Sea shelf and its influence on the biological process (in Chinese) [dissertation]. Qingdao: Institute of Oceanology, Chinese Academy of Sciences, 116

Yang Dezhou, Huang Ruixin, Yin Baoshu, et al. 2018. Topographic beta spiral and onshore intrusion of the Kuroshio Current. Geophysical Research Letters, 45(1): 287–296, doi: 10.1002/2017GL076614

Yang Dezhou, Yin Baoshu, Liu Zhiliang, et al. 2011. Numerical study of the ocean circulation on the East China Sea shelf and a Kuroshio bottom branch northeast of Taiwan in summer. Journal of Geophysical Research: Oceans, 116(C5): C05015

Yu Long, Xiong Xuejun, Guo Yanliang, et al. 2014. Analysis of the path and axis features of the Kuroshio at the depth of 15m based on drifting buoy data. Advances in Marine Science (in Chinese), 32(3): 316–323

Yu Fei, Zang Jiaye, Guo Binghuo, et al. 2002. Some phenomena of the Kuroshio Intrusion Into shelf area and the shelf circulation of the East China Sea. Advances in Marine Science (in Chinese), 20(3): 21–28

Zeng Dingyong, Ni Xiaobo, Huang Daji. 2012. Temporal and spatial variability of the ZheMin coastal current and the Taiwan warm current in winter in the southern Zhejiang coastal sea. Science in China Series: Earth Sciences (in Chinese), 42(7): 1123–1134

Zhang Yansheng, Yu Fei, Si Guangcheng. 2017. Seasonal variation of cold vortex northeast of Diaoyu Island. Oceanologia et Limnologia Sinica (in Chinese), 48(3): 454–464

Zhao Ruixiang, Liu Zhiliang. 2014. The seasonal variation of the Kuroshio subsurface water intrusion northeast of Taiwan. Haiyang Xuebao (in Chinese), 36(1): 20–27

Zhou Peng, Song Xiuxian, Yuan Yongquan, et al. 2018. Intrusion of the Kuroshio Subsurface Water in the southern East China Sea and its variation in 2014 and 2015 traced by dissolved inorganic iodine species. Progress in Oceanography, 165: 287–298, doi: 10.1016/j.pocean.2018.06.011